

Measurement of the Branching Ratio and Form Factor of $K_L \rightarrow \mu^+ \mu^- \gamma$

A. Alavi-Harati,¹² T. Alexopoulos,¹² M. Arenton,¹¹ K. Arisaka,² S. Averitte,¹⁰ A. R. Barker,⁵ L. Bellantoni,⁷ A. Bellavance,⁹ J. Belz,¹⁰ R. Ben-David,⁷ D. R. Bergman,¹⁰ E. Blucher,⁴ G. J. Bock,⁷ C. Bown,⁴ S. Bright,⁴ E. Cheu,¹ S. Childress,⁷ R. Coleman,⁷ M. D. Corcoran,⁹ G. Corti,¹¹ B. Cox,¹¹ M. B. Crisler,⁷ A. R. Erwin,¹² R. Ford,⁷ A. Glazov,⁴ A. Golossanov,¹¹ G. Graham,⁴ J. Graham,⁴ K. Hagan,¹¹ E. Halkiadakis,¹⁰ J. Hamm,¹ K. Hanagaki,⁸ S. Hidaka,⁸ Y. B. Hsiung,⁷ V. Jejer,¹¹ D. A. Jensen,⁷ R. Kessler,⁴ H. G. E. Kobrak,³ J. LaDue,⁵ A. Lath,¹⁰ A. Ledovskoy,¹¹ P. L. McBride,⁷ P. Mikelsons,⁵ E. Monnier,⁴ T. Nakaya,⁷ K. S. Nelson,¹¹ H. Nguyen,⁷ V. O'Dell,⁷ M. Pang,⁷ R. Pordes,⁷ V. Prasad,⁴ B. Quinn,^{4,*} E. J. Ramberg,⁷ R. E. Ray,⁷ A. Roodman,⁴ M. Sadamoto,⁸ S. Schnetzer,¹⁰ K. Senyo,⁸ P. Shanahan,⁷ P. S. Shawhan,⁴ J. Shields,¹¹ W. Slater,² N. Solomey,⁴ S. V. Somalwar,¹⁰ R. L. Stone,¹⁰ E. C. Swallow,^{4,6} S. A. Taegar,¹ R. J. Tesarek,¹⁰ G. B. Thomson,¹⁰ P. A. Toale,⁵ A. Tripathi,² R. Tschirhart,⁷ S. E. Turner,² Y. W. Wah,⁴ J. Wang,¹ H. B. White,⁷ J. Whitmore,⁷ B. Winstein,⁴ R. Winston,⁴ T. Yamanaka,⁸ and E. D. Zimmerman⁴

(KTeV Collaboration)

¹University of Arizona, Tucson, Arizona 85721

²University of California at Los Angeles, Los Angeles, California 90095

³University of California at San Diego, La Jolla, California 92093

⁴The Enrico Fermi Institute, The University of Chicago, Chicago, Illinois 60637

⁵University of Colorado, Boulder, Colorado 80309

⁶Elmhurst College, Elmhurst, Illinois 60126

⁷Fermi National Accelerator Laboratory, Batavia, Illinois 60510

⁸Osaka University, Toyonaka, Osaka 560-0043 Japan

⁹Rice University, Houston, Texas 77005

¹⁰Rutgers University, Piscataway, New Jersey 08854

¹¹The Department of Physics and Institute of Nuclear and Particle Physics, University of Virginia, Charlottesville, Virginia 22901

¹²University of Wisconsin, Madison, Wisconsin 53706

(Received 30 January 2001; published 26 July 2001)

We report on the analysis of the rare decay $K_L \rightarrow \mu^+ \mu^- \gamma$ the 1997 data from the KTeV experiment at Fermilab. A total of 9327 candidate events are observed with 2.4% background, representing a factor of 40 increase in statistics over the current world sample. We find that $B(K_L \rightarrow \mu^+ \mu^- \gamma) = (3.62 \pm 0.04_{\text{stat}} \pm 0.08_{\text{sys}}) \times 10^{-7}$. The form factor parameter α_{K^*} is measured to be $\alpha_{K^*} = -0.160^{+0.026}_{-0.028}$. In addition, we make the first measurement of the parameter α from the D'Ambrosio-Isidori-Portolés form factor, finding $\alpha = -1.54 \pm 0.10$. In that model, this α measurement limits the Cabibbo-Kobayashi-Maskawa parameter $\rho > -0.2$.

DOI: 10.1103/PhysRevLett.87.071801

PACS numbers: 13.20.Eb, 12.15.Hh, 14.40.Aq

The $K_L \rightarrow \mu^+ \mu^-$ decay is a probe into the long-distance electromagnetic physics associated with the intermediate $K_L \rightarrow \gamma^* \gamma$ vertex. Long-distance contributions related to those in $K_L \rightarrow \mu^+ \mu^- \gamma$ dominate the $K_L \rightarrow \mu^+ \mu^-$ rate, which also receives small contributions from short-distance weak processes sensitive to the Cabibbo-Kobayashi-Maskawa (CKM) parameter ρ [1,2]. Therefore, an understanding of long-distance physics in

$K_L \rightarrow \mu^+ \mu^- \gamma$ may provide a chance to test the standard model using $K_L \rightarrow \mu^+ \mu^-$.

A high-precision measurement of $B(K_L \rightarrow \mu^+ \mu^- \gamma)$ is presented in this Letter. The $K_L \rightarrow \mu^+ \mu^- \gamma$ signal and $K_L \rightarrow \pi^+ \pi^- \pi^0$, $\pi^0 \rightarrow \gamma \gamma$ normalization data were collected in 1997 by the KTeV experiment at Fermilab. Also presented are measurements of long-distance form factors according to the models of Bergström, Massó, and Singer (BMS) [3]

$$f(x) = \frac{1}{1 - 0.418x} + \frac{C \alpha_{K^*}}{1 - 0.308x} \left(\frac{4}{3} - \frac{1}{1 - 0.418x} - \frac{1}{9} \frac{1}{1 - 0.405x} - \frac{2}{9} \frac{1}{1 - 0.238x} \right), \quad (1)$$

and of D'Ambrosio, Isidori, and Portolés (DIP) [4]

$$f(x) = 1 + \alpha \left(\frac{x}{x - 2.40} \right), \quad (2)$$

where $x = (m_{\mu\mu}/m_{K_L})^2$ and C is a dimensionless constant [5]. Each model of the $\gamma^* \gamma$ form factor includes a single free parameter: α_{K^*} for BMS and α for DIP. These parameters can be determined from the differential and integrated

decay rates (i.e., from the dimuon mass distribution and the branching ratio).

KTeV utilized kaon beams produced by 800 GeV protons incident on a BeO target. A series of absorbers, magnetic sweepers, and collimators created two beams that entered a vacuum decay region extending from 94 to 159 m downstream of the target. A charged-particle spectrometer

consisting of four drift chambers and an analysis magnet followed the vacuum region. The horizontal and vertical position resolutions of the chambers were $\sim 100 \mu\text{m}$, and the momentum resolution was $\sigma(P)/P = 0.38\% \oplus 0.016\%P$, with P in GeV/c . Two trigger hodoscope planes preceded the electromagnetic calorimeter which consisted of 3100 pure CsI crystals. The calorimeter (CsI) energy resolution was $\sigma(E)/E = 0.45\% \oplus 2\%/\sqrt{E}$, with E in GeV , and the position resolution was $\sim 1 \text{ mm}$. A photon veto system detected particles leaving the fiducial region of the detector.

Behind the CsI, a muon filter with 10 cm of lead and 511 cm of steel comprised 31 interaction lengths. Over 99% of muons with momenta greater than $10 \text{ GeV}/c$ passed through the filter. The probability of charged pion punch-through (including decay downstream of the CsI) increased with momentum, and on average was $\sim 0.5\%$. A pair of $3 \times 3 \text{ m}^2$ scintillator planes (MU3) located just behind the muon filter was used to identify muons. MU3 consisted of one horizontal and one vertical plane, each with 15 cm segmentation. Further details of the KTeV detector can be found elsewhere [6,7].

A $K_L \rightarrow \mu^+ \mu^- \gamma$ event appears as two oppositely charged tracks that originate from a single vertex and point to small energy deposits in the CsI, two hits in each plane of MU3, and an additional energy shower in the CsI not associated with a track. All of the backgrounds are kaon decays with one or more final-state charged pions that are misidentified as muons. The dominant background mode is $K_L \rightarrow \pi^\pm \mu^\mp \nu$ ($K_{\mu 3}$) with the pion either decaying in flight or punching through to MU3 and additional CsI energy accidentally coincident with the kaon decay. Smaller contributions come from $K_L \rightarrow \pi^\pm \mu^\mp \nu \gamma$ ($K_{\mu 3\gamma}$) and $K_L \rightarrow \pi^+ \pi^- \pi^0$.

The fact that there are no muons in the $K_L \rightarrow \pi^+ \pi^- \pi^0$ normalization mode necessitates a very good understanding of the absolute efficiency for muon detection. Monte Carlo simulations of muon transport based on GEANT were calibrated using data from muon beams produced with special absorber and magnet configurations. The agreement in the muon momentum threshold and multiple scattering is excellent (Fig. 1), and the muon efficiency has been measured to $< 0.5\%$ of itself.

Signal and normalization data were collected with separate triggers. Both required hits in the trigger hodoscopes and drift chambers consistent with two tracks pointing to clusters in the CsI and originating from a common vertex. The signal trigger also required that each MU3 plane have at least two hits, clusters matched to tracks have less than 5 GeV , and there be at least one cluster over 1 GeV not matched to a track. The normalization trigger was prescaled by a factor of 7000.

The offline reconstruction of $K_L \rightarrow \mu^+ \mu^- \gamma$ events required that tracks have sufficient momentum to penetrate the muon filter ($> 10 \text{ GeV}/c$) and be matched to minimum-ionizing energy deposits in the CsI ($< 1 \text{ GeV}$). At least one of the MU3 planes had to have nonadjacent hits in order

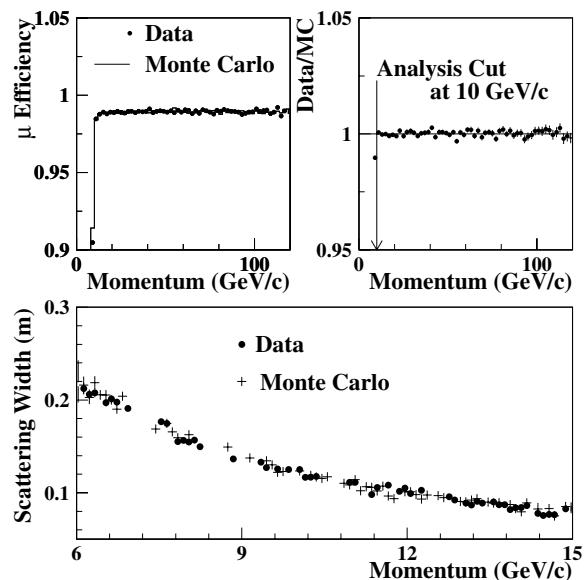


FIG. 1. Muon detection efficiency vs track momentum (top left), data to Monte Carlo ratio of muon efficiency (top right), and multiple scattering width vs track momentum (bottom). Widths are those of Gaussian fits to the difference between extrapolated track position and hit counter position.

to eliminate events with only one muon and a δ ray. The reconstructed position of the vertex was required to be between 97 and 157 m from the target and within the transverse beam dimensions. Kaon momenta had to reconstruct between 20 and 220 GeV/c . The separation between a track position at the CsI and the position of its matched cluster was required to be less than 3.5 cm, and unmatched photon cluster positions had to be at least 20 cm away from clusters matched to tracks.

Cutting events with a photon energy less than 8 GeV eliminated half of the $K_{\mu 3}$ background and a significant number of $K_{\mu 3\gamma}$ and $K_L \rightarrow \pi^+ \pi^- \pi^0$ decays. Two-thirds of the remaining $K_{\mu 3}$ events were removed by requiring that the transverse energy distribution of the photon cluster be consistent with deposition from a single photon. A further 38% of $K_{\mu 3}$'s was rejected by cutting poorly reconstructed vertices resulting from extra drift chamber hits or kinked tracks from π^\pm decays. Requiring that upstream and downstream track segments match within 1 mm at the magnet bend plane removes about half of the $K_L \rightarrow \pi^+ \pi^- \pi^0$ background. Less than 0.5% of the total remaining background survived the cut that the reconstructed transverse momentum relative to the kaon flight direction (P_\perp) be less than 10 MeV/c . The P_\perp cut is extremely effective because all backgrounds are characterized by missing or extra momentum.

Reconstruction of the normalization mode was identical to that of the signal in all ways except the following: it did not require MU3 hits, required two photon clusters with a reconstructed mass of $135 \pm 10 \text{ MeV}/c^2$, reduced the photon energy cut to 3 GeV , cut events with a ratio of cluster energy to track momentum greater than 0.9 (rather

than cut on the cluster energy), and rejected events with tracks extrapolating within 2.5 cm of the CsI beam holes.

The final reconstructed $m_{\mu^+\mu^- \gamma}$ distribution is shown in Fig. 2. There are 9327 events in the mass window $490 < m_{\mu^+\mu^- \gamma} < 506 \text{ MeV}/c^2$. The Monte Carlo reproduces the mass distribution extremely well over a wide range and predicts 221.9 ± 14.9 background events under the signal mass peak. Pion decay and punch through each account for about half of the total background. The background estimation was checked by extrapolating high- P_{\perp} data into the signal region (220 ± 6 events) and by performing a simple fit to the mass distribution (215 ± 15 events). The final $K_L \rightarrow \pi^+\pi^-\pi^0$ sample is background free and contains 210 660 events. Monte Carlo acceptances for the signal and normalization are $(7.895 \pm 0.018)\%$ and $(3.735 \pm 0.003)\%$, respectively. The ratio $B(K_L \rightarrow \mu^+\mu^-\gamma)/[B(K_L \rightarrow \pi^+\pi^-\pi^0)B(\pi^0 \rightarrow \gamma\gamma)] = (2.92 \pm 0.03_{\text{stat}}) \times 10^{-6}$ is measured from these data and acceptances.

Several possible sources of systematic error in the acceptance ratio were studied. The MU3 crack sizes and muon filter thickness in the Monte Carlo were varied over the range of survey data uncertainty. Significant error contributions came from the scale of drift chamber inefficiency simulations, the P_{\perp} cut placement, and residual trigger bias. The signal acceptance is fairly insensitive to the choice of the form factor parameter, the values of which were varied over the range of previously reported results. These and other uncertainties are listed in Table I. The error on $B(K_L \rightarrow \pi^+\pi^-\pi^0)$ dominates the total systematic error, which is used with the normalization branching ratios [8] to obtain the final result $B(K_L \rightarrow \mu^+\mu^-\gamma) = (3.62 \pm 0.04_{\text{stat}} \pm 0.08_{\text{syst}}) \times 10^{-7}$. This

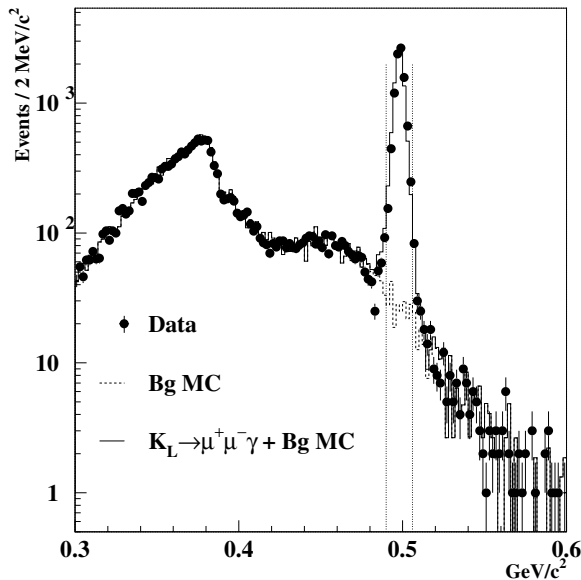


FIG. 2. The reconstructed $m_{\mu^+\mu^- \gamma}$ distribution after final cuts. The large peak centered at $380 \text{ MeV}/c^2$ is $K_L \rightarrow \pi^+\pi^-\pi^0$. $K_{\mu 3}$ dominates the background from $\sim 400 \text{ MeV}/c^2$ out to $600 \text{ MeV}/c^2$ with a slight enhancement at $450 \text{ MeV}/c^2$ from $K_{\mu 3\gamma}$.

071801-3

TABLE I. Systematic errors.

Source	$B(K_L \rightarrow \mu^+\mu^-\gamma)$ Uncertainty
MU3 crack simulation	0.5%
Muon filter thickness	0.4%
dc inefficiency simulation	0.5%
Photon energy uncertainty	0.1%
P_{\perp} cut	0.6%
Track momentum cut	0.2%
Trigger bias	0.8%
Background uncertainty	0.2%
Monte Carlo statistics	0.2%
Monte Carlo form factor	0.4%
Total internal syst. error	1.4%
$B(K_L \rightarrow \pi^+\pi^-\pi^0)$	1.6%
Total	2.1%

represents more than a factor of 3 improvement in precision over previous measurements [8].

Figure 3 shows a model-independent measurement of the form factor as a function of x (bin-by-bin values for $|f(x)|^2$ are given in [9]). The model parameters α_{K^*} and α were measured from the shape of the x distribution by making an unbinned likelihood comparison with Monte Carlo generated with various parameter values (Fig. 4). In this way, the parameters were measured to be $\alpha_{K^*}^{\text{shape}} = -0.193^{+0.035}_{-0.049}$ and $\alpha^{\text{shape}} = -1.73^{+0.14}_{-0.18}$, where systematic errors dominated by the placement of the cut on track momentum are included. Integrating the differential decay rate using Eqs. (1) or (2), $B(K_L \rightarrow \mu^+\mu^-\gamma)$ was found as a function of α_{K^*} or α , yielding $\alpha_{K^*}^{\text{BR}} = -0.117 \pm 0.040$ and $\alpha^{\text{BR}} = -1.38 \pm 0.13$. The shape and branching ratio measurements were combined to give $\alpha_{K^*} = -0.160^{+0.026}_{-0.028}$ and $\alpha = -1.54 \pm 0.10$.

The self-consistency of each model was checked by comparing shape and branching ratio parameter measurements. The differences of 1.2σ for BMS and 1.6σ

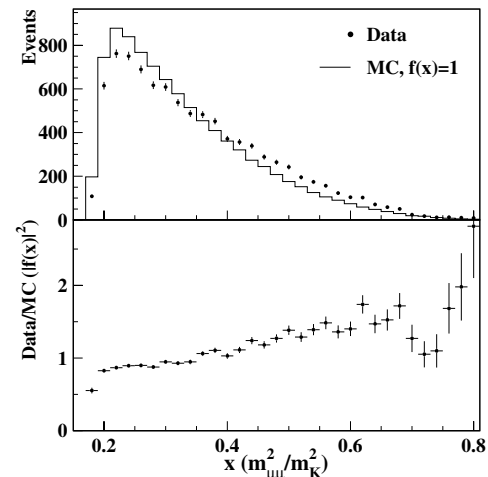


FIG. 3. The dimuon mass distributions for data and for Monte Carlo with no form factor (top). The data/Monte Carlo ratio is a direct measurement of the form factor (bottom). The Monte Carlo is normalized to the total number of data events.

071801-3

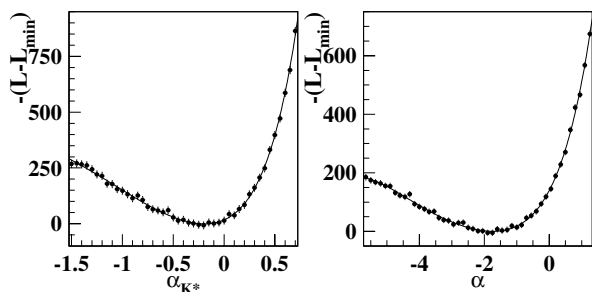


FIG. 4. Log-likelihood fits to the BMS parameter α_{K^*} (left), and to the DIP parameter α (right).

for DIP give no clear distinction. BMS predict $|\alpha_{K^*}| = 0.25 \pm 0.05$ and equivalently $B(K_L \rightarrow \mu^+ \mu^- \gamma) = (4.11 \pm 0.18) \times 10^{-7}$, which is 2.1σ higher than the measured rate (DIP make no predictions of α). Also, Fig. 5 shows α_{K^*} measurements from $K_L \rightarrow e^+ e^- \gamma$ and $K_L \rightarrow \mu^+ \mu^- \gamma$ [10,11]. There is now a 3σ difference between muon and electron mode measurements of α_{K^*} .

Extraction of a ρ limit begins with the decomposition $B(K_L \rightarrow \mu^+ \mu^-) = |\text{Re}A|^2 + |\text{Im}A|^2$. $|\text{Im}A|^2$ is the long-distance unitarity bound and corresponds to the case of two real intermediate photons. The experimental value $B(K_L \rightarrow \mu^+ \mu^-) = (7.15 \pm 0.16) \times 10^{-9}$ is almost completely saturated by the unitarity bound calculated to be $|\text{Im}A|^2 = (7.00 \pm 0.18) \times 10^{-9}$ [8,12]. Short-distance and $K_L \rightarrow \gamma^* \gamma^*$ contributions make up $\text{Re}A = \text{Re}A_{\text{SD}} + \text{Re}A_{\text{LD}}$, which is limited to $|\text{Re}A_{\text{exp}}|^2 < 4.0 \times 10^{-10}$ (90% C.L.). $\text{Re}A_{\text{LD}}$ can be calculated using the form factor measured from $K_L \rightarrow \mu^+ \mu^- \gamma$, and ρ is limited with the expression

$$\bar{\rho} > 1.2 - \max \left[\frac{|\text{Re}A_{\text{exp}}| + |\text{Re}A_{\text{LD}}|}{3 \times 10^{-5}} \left(\frac{\bar{m}_l(m_l)}{170 \text{ GeV}} \right)^{-1.55} \times \left(\frac{|V_{cb}|}{0.040} \right)^{-2} \right], \quad (3)$$

where $\bar{\rho} = \rho(1 - \lambda^2/2)$ [4,13].

Using the measured form factor parameters, the limits on $\text{Re}A_{\text{LD}}$ derived with the two models are $|\text{Re}A_{\text{LD}}|_{\text{BMS}} < 3.6 \times 10^{-5}$ and $|\text{Re}A_{\text{LD}}|_{\text{DIP}} < 2.14 \times 10^{-5}$. $|\text{Re}A_{\text{LD}}|_{\text{BMS}}$ is essentially a true upper bound [14] and is added algebraically to the limit on $|\text{Re}A_{\text{exp}}|$ to obtain $\rho > -1.0$. In forming the $|\text{Re}A_{\text{exp}}| + |\text{Re}A_{\text{LD}}|_{\text{DIP}}$ limit, the measured values of $|\text{Re}A_{\text{exp}}|^2$ and $|\text{Re}A_{\text{LD}}|_{\text{DIP}}$ are converted into Gaussian distributions, the product of which forms a two-dimensional probability distribution. The contour of $|\text{Re}A_{\text{exp}}| + |\text{Re}A_{\text{LD}}|_{\text{DIP}}$ under which 90% of the probability in the positive (physical) quadrant lies determines the limit. This procedure yields the result $\rho > -0.2$, which is close to the combined limit of $\rho > 0$ from $|V_{ub}|$, B mixing, and ϵ [15]. With the current precision of K_L decay measurements, ρ limits from the $K_L \rightarrow \gamma^* \gamma$ channel are dominated by theoretical uncertainties, which may be difficult to control [16]. Also, inconsistencies in α_{K^*} and α results point to possible

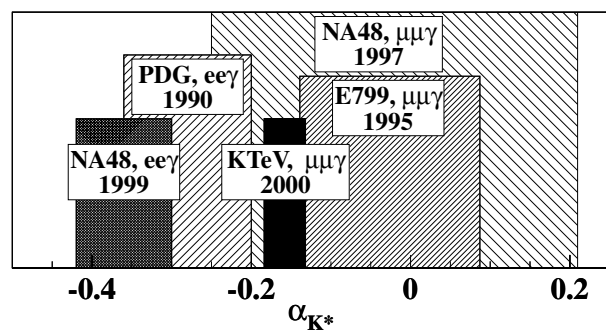


FIG. 5. Comparison of the α_{K^*} measurement with previous experiments. The PDG value includes measurements from the BNL845 and NA31 experiments.

deficiencies in the form factor models. At the current level of theoretical understanding, the remaining experimental need is an α measurement from $K_L \rightarrow e^+ e^- \gamma$ to provide a consistency check of the DIP model.

We gratefully acknowledge the support and effort of the Fermilab staff and the technical staffs of the participating institutions for their vital contributions. This work was supported in part by the U.S. Department of Energy, The National Science Foundation, and The Ministry of Education and Science of Japan.

*To whom correspondence should be addressed.

- [1] G. Bélanger and C. Q. Geng, Phys. Rev. D **43**, 140 (1991); J. L. Ritchie and S. G. Wojcicki, Rev. Mod. Phys. **65**, 1149 (1993).
- [2] L. Wolfenstein, Phys. Rev. Lett. **51**, 1945 (1983).
- [3] L. Bergström, E. Massó, and P. Singer, Phys. Lett. **131B**, 229 (1983).
- [4] G. D'Ambrosio, G. Isidori, and J. Portolés, Phys. Lett. B **423**, 385 (1998).
- [5] References [10,11] use the value $C = 2.5$ calculated with numbers from the 1988 Particle Data Group. Here we use $C = 2.3$ based on information found in [8].
- [6] A. Alavi-Harati *et al.*, Phys. Rev. Lett. **83**, 922 (1999).
- [7] A. Alavi-Harati *et al.*, Phys. Rev. D **61**, 072006 (2000).
- [8] Particle Data Group, D. E. Groom *et al.*, Eur. Phys. J. C **15**, 514 (2000).
- [9] B. Quinn, Ph.D. thesis, The University of Chicago, 2000.
- [10] G. D. Barr *et al.*, Phys. Lett. B **240**, 283 (1990); K. E. Ohl *et al.*, Phys. Rev. Lett. **65**, 1407 (1990); V. Fanti *et al.*, Phys. Lett. B **458**, 553 (1999).
- [11] M. B. Spencer *et al.*, Phys. Rev. Lett. **74**, 3323 (1995); V. Fanti *et al.* Z. Phys. C **76**, 653 (1997).
- [12] L. M. Sehgal, Phys. Rev. **183**, 1511 (1969).
- [13] A. J. Buras and R. Fleischer, in *Heavy Flavours II*, edited by A. J. Buras and M. Lindner (World Scientific, Singapore, 1997), p. 166.
- [14] L. Bergström *et al.*, Phys. Lett. **134B**, 373 (1984).
- [15] A. Ali and D. London, in Proceedings of the 3rd Workshop on Physics and Detectors for DAPHNE, Frascati, Italy, 1999 (hep-ph/0002167).
- [16] G. Valencia, Nucl. Phys. **B517**, 339 (1998); M. Knecht *et al.*, Phys. Rev. Lett. **83**, 5230 (1999).